A&A 433, 1063–1077 (2005)
DOI: 10.1051/0004-6361:20042066

Astronomy & Astrophysics

First detections of the cataclysmic variable AE Aquarii in the near to far infrared with ISO⋆ and IRAS⋆⋆: Investigating the various possible thermal and non-thermal contributions

M. Abada-Simon[1], J. Casares[2], A. Evans[3], S. Eyres[4], R. Fender[5], S. Garrington[6], O. de Jager[7], N. Kuno[8], I. G. Martínez-Pais[2], D. de Martino[9], H. Matsuo[8], M. Mouchet[10,11], G. Pooley[12], G. Ramsay[13], A. Salama[14], and B. Schulz[14,15]

[1] LESIA/CNRS UMR8109, Observatoire de Paris, 92195 Meudon, France; e-mail: meil.abada-simon@obspm.fr
[2] Instituto de Astrofísica de Canarias, Tenerife, Spain
[3] Astrophysics Group, Keele University, UK
[4] University of Central Lancashire, Preston, UK
[5] University of Amsterdam, The Netherlands
[6] MERLIN/VLBI National Facility, Jodrell Bank Observatory, Macclesfield, UK
[7] Potchefstroom University, South Africa
[8] Nobeyama Radio Observatory, Japan
[9] Osservatorio Astronomico di Capodimonte, Napoli, Italy
[10] Université D. Diderot/Paris 7, Paris, France
[11] LUTH/CNRS UMR8102, Observatoire de Paris, Meudon, France
[12] Cavendish Laboratory, Cambridge, UK
[13] Mullard Space Science Lab, University College London, UK
[14] ISO Data Centre, Astrophysics Division, ESA, Madrid, Spain
[15] California Institute of Technology, Pasadena, USA

Received 12 November 2001 / Accepted 16 December 2004

Abstract. We have used ISO to observe the Magnetic Cataclysmic Variable AE Aquarii in the previously unexplored range from 4.8 μm up to 170 μm in the framework of a coordinated multi-wavelength campaign from the radio to optical wavelengths. We have obtained for the first time a spectrum between 4.8 and 7.3 μm with ISOCAM and ISOPHOT-P: the major contribution comes from the secondary star spectrum, with some thermal emission from the accretion stream, and possibly some additional cyclotron radiation from the post-shock accretion material close to the magnetised white dwarf. Having re-processed ISOPHOT-C data, we confirm AE Aqr detection at 90 μm and we have re-estimated its upper limit at 170 μm. In addition, having re-processed IRAS data, we have detected AE Aqr at 60 μm and we have estimated its upper limits at 12, 25, and 100 μm. The literature shows that the time-averaged spectrum of AE Aqr increases roughly with frequency from the radio wavelengths up to ~761 μm; our results indicate that it seems to be approximately flat between ~761 and ~90 μm, at the same level as the 3σ upper limit at 170 μm; and it then decreases from ~90 μm to ~7 μm. Thermal emission from dust grains or from a circum-binary disc seems to be very unlikely in AE Aqr, unless such a disc has properties substantially different from those predicted recently. Since various measurements and the usual assumptions on the source size suggest a brightness temperature below 10^9 K at $\lambda \leq 3.4$ mm, we have reconsidered also the possible mechanisms explaining the emission already known from the submillimetre to the radio. The complex average spectrum measured from ~7 μm to the radio must be explained by emission from a plasma composed of more than one "pure" non-thermal electron energy distribution (usually assumed to be a power-law): either a very large volume (diameter $\geq$ 80 times the binary separation) could be the source of thermal bremsstrahlung which would dominate from ~10 μm to the ~millimetre, with, inside, a non-thermal source of synchrotron which dominates in radio; or, more probably, an initially small infrared source composed of several distributions (possibly both thermal, and non-thermal, mildly relativistic electrons) radiates gyro-synchrotron and expands moderately: it requires to be re-energised in order to lead to the observed, larger, radio source of highly relativistic electrons (in the form of several non-thermal distributions) which produce synchrotron.

Key words. stars: novae, cataclysmic variables – infrared: stars – radio continuum: stars – stars: flare – radiation mechanisms: thermal – radiation mechanisms: non-thermal

⋆ Based on observations with the Infrared Satellite Observatory (ISO), an ESA project with instruments funded by ESA Member States (especially the PI countries: France, Germany, The Netherlands and the UK) and with the participation of ISAS and NASA.

⋆⋆ The Infra-Red Astronomical Satellite (IRAS) mission was a collaborative effort by the USA (NASA), The Netherlands (NIVR), and the UK (SERC).

1. Introduction

1.1. General presentation

Among the large number of astrophysical sources in which accretion occurs, Cataclysmic Variables (CVs) are perhaps the most useful to study accretion since many of their system parameters, such as distance, magnetic field, and emission mechanisms, can be determined. AE Aquarii is a peculiar member of the magnetic CV (MCV) sub-class of interacting binaries. MCVs consist of a white dwarf whose magnetic field strength is strong enough ($\geq 10^5$ G) to influence the accretion flow from the Roche-Lobe overfilling late type companion star. Generally the secondary stars in CVs are of M type, while in AE Aqr the companion is of spectral type K5V, thus suggesting an evolved or a different binary evolution path for this system (e.g. Welsh et al. 1995, hereafter WHG, and Schenker et al. 2002). In AE Aqr, the white dwarf surface magnetic field strength is estimated to be $10^4 \leq B_{\rm wd}({\rm G}) \leq 10^7$ (Lamb & Patterson 1983; Lamb 1988; Stockman et al. 1992), and its angle with the rotation axis is $\sim 70^\circ$ (Eracleous et al. 1994). The system is non eclipsing, with an inclination angle $i = 55 \pm 7^\circ$ (WHG). The red star contribution to the continuum emission in the range 6000−7000 Å is ∼95% of the quiescent flux (Casares et al. 1996). HIPPARCOS gives a distance to AE Aqr of 79−144 pc, 102 pc being the most probable value (Perryman et al. 1997), which will be used in the discussion and interpretation section.

AE Aqr displays flux variations on timescales from seconds to days, from radio to soft X-rays. Moreover, AE Aqr exhibits a number of unique properties. The spin period (33.08 s) of the white dwarf is the second fastest of any CV (Patterson 1979), which makes AE Aqr the most asynchronous system with its orbital period ($P_{\rm orb}$ = 9.88 h), and thus a strong candidate for a "propeller": it is thought that no accretion disc is formed around the white dwarf, most of the accreting material being expelled from the system (Wynn et al. 1997, hereafter WKH97). Unusually for a CV, there have been several independent detections of high energy X-rays and of TeV γ-rays, which tend to emphasize the close relation between AE Aqr and X-ray binaries (Bowden et al. 1992; Meintjes et al. 1992, 1994); a fraction of the white dwarf spindown power, which exceeds the accretion power, may contribute to the acceleration of particles, which may explain the radio and the γ-ray emissions (de Jager et al. 1994). Because of its brightness (V = 10−12), AE Aqr is an excellent system to test models of interaction between a plasma and a rapidly rotating magnetic field.

1.2. The near-to-far infrared emission of AE Aqr

Szkody (1977) obtained photometry of AE Aqr in the U, B, V, r (0.68 μm), R2 (0.81 μm), J (1.25 μm), H (1.65 μm), K (2.2 μm) and L (3.4 μm) bands, and found a peak in the r band. Szkody (1977) found that the secondary dominates over the accretion stream, but does not have a typical K-type star spectrum: there is some evidence for a hotter component. Tanzi et al. (1981) also performed broad-band infrared (IR) observations of AE Aqr from 1.25 to 3.4 μm (J, H, K and L bands) suggesting that the secondary was a K5V star. In order to estimate the proportion of near[1] infrared light in CVs which is supplied by the red dwarf with respect to the accretion stream and disc, Berriman et al. (1985, hereafter BSC85) compiled published and unpublished *JHK* photometry observations. While they concluded that *JHK* photometry is not a good probe of the red dwarfs, they did estimate a minimum distance (of 90 pc) and a K star of 0.9 solar radius. Dhillon & Marsh (1995) obtained infrared spectra of AE Aqr in the 1.0−2.5 μm range, revealing absorption features of the secondary star as well as strong hydrogen emission lines.

Dust grains can give thermal emission from 1 to 100 μm. BSC85 obtained a 3σ upper limit of 40.5 mJy[2] at 10 μm. In addition, AE Aqr was not detected by IRAS in 1983: preliminary upper limits of 1 Jy at 100 μm, and 200 mJy at 12, 25 and 60 μm (IRAS archive) had been obtained through a first automatic data processing. These five non-detections suggested that there is little evidence for dust being present in AE Aqr.

Another possible source of substantial emission at $\lambda >$ 1 μm is a Circum-Binary (CB) disc of effective temperatures between ≤30 K (outermost part) and 3000 K (inner part) extending up to several astronomical units (Dubus et al. 2002, hereafter DTS): at the distance of AE Aqr, a typical flux of about 300 mJy at 10 μm would be expected, which is far above the upper limit obtained by BSC85, so the flux could be variable with time and/or the CB disc could have parameters different from those predicted by DTS. Such a disc is expected to cause accelerated mass transfer at a rate $\geq 10^{-8} M_{\rm sun}$/yr, but in AE Aqr, the estimated accretion rate is a factor $\sim 10^4$ smaller (WKH97). Very recently, flares have been observed at 11.7 and 17.6 μm: they cannot be attributed to a thermal emission process (Dubus et al. 2004).

1.3. Origin of AE Aqr radio to sub-millimetre emission

The radio emission detected in AE Aqr, firstly by Bookbinder & Lamb (1987), and in one other MCV (AM Her) was considered as the first indirect evidence for the presence of a strong magnetic field on the secondary star (Chanmugam 1987). This may have implications for the evolution of CVs through magnetic braking by the secondary (Li et al. 1995, and references therein). However, most MCVs are not detected in radio: is it because they emit radio emission below the detection threshold of the presently available instruments, or is a strong magnetic field on both the white dwarf and the red component necessary and sufficient to get radio flares (via field line reconnections)? Most of them have not been observed over sufficiently long periods of time to have reasonable chances to detect at least the peak of a flare.

The origin of AE Aqr radio flares remains unclear; a total of only 5 h of simultaneous observations suggest that the optical and radio flares are not correlated, therefore not due to the same

[1] In this paper, we use "near infrared" up to ∼7 μm, "mid infrared" for $7 \leq \lambda(\mu{\rm m}) \leq 90$, "far infrared" for $90 \leq \lambda(\mu{\rm m}) \leq 500$, "sub-millimetre" for $0.5 \leq \lambda({\rm mm}) \leq 1$, "millimetre" for 1 mm $\leq \lambda \leq$ 1 cm, and "radio" for $\lambda \geq 1$ cm.

[2] In this paper, we use flux densities – written S_ν at frequency ν – in milli-Jansky – 1 mJy = 10^{-26} erg/cm^2/s/Hz.

process, but this needs to be confirmed over at least one orbital period; furthermore they cannot be attributed to the K star alone since they are not periodic, and similar K stars do not flare as much as AE Aqr (Abada-Simon et al. 1995a). Uninterrupted observations of AE Aqr at 3.6 cm for ~10 h with a 3 s time resolution confirmed that the radio emission shows no sign of the presence of coherent oscillations at the white dwarf spin period, or quasi-periodic oscillations (QPOs) (Bastian et al. 1996). On the other hand, the 33 s periodicity observed in quiescence in the soft X-rays and ultra-violet implies that these emissions are produced close to the white dwarf.

The observed radio emission of AE Aqr is the strongest among CVs, and it is almost always detectable, in the form of flares of various amplitudes on time scales ranging between several tens of seconds to hours. Assuming that the radio source is a sphere of radius r (in cm) emitting isotropically, the brightness temperature is given by the Rayleigh-Jeans approximation of the Planck law, which can be written, at the distance of 102 pc (for AE Aqr):

$$T_{\rm b}({\rm K}) \simeq 10^{51} \times \frac{S_\nu}{(\nu r)^2} \quad (1)$$

where S_ν is the flux density in mJy, and ν the observing frequency in Hz. (These same assumptions are kept in all this paper to estimate values of $T_{\rm b}$.) If the source diameter $2r$ is not larger than the binary separation ($a \simeq 1.8 \times 10^{11}$ cm), then the brightness temperature of AE Aqr is high ($\geq 10^{10}$ K at $\lambda \geq 1$ cm), which implies that the radio emission is non thermal. Further it is not highly polarized (<10%), with a very wide bandwidth ($\Delta f \simeq 2f$), and exhibits no fast time variation ($\delta t \geq 10$ s): all these characteristics suggest that the emission is incoherent (Bastian et al. 1985, hereafter BDC).

BDC, who observed AE Aqr in radio four times between October 1985 and January 1987, suggested that AE Aqr may be a low-power analogue to the X-ray binary Cyg X-3 (Newell et al. 1998). Indeed, since they observed that the daily time-averaged spectra of AE Aqr increase with frequency (power-law $S_\nu = S_o \nu^\alpha$ of spectral index $\alpha \simeq 0.4$–0.6), they suggested that the radio flares ($\lambda = 1$–21 cm) may be caused by the superposition of optically thick synchrotron radiation from plasma clouds of relativistic electrons with a Lorentz factor $\gamma \simeq 3$–30 – which one assumed to have a power-law energy distribution ($N(E) \propto E^{-\delta}$) – and ejected from the binary. Indeed, if the electron energy distribution function is a power-law of spectral index $-\delta$, the synchrotron optically thin emitted flux density is also a power-law, of spectral index $-(\delta - 1)/2$, which implies a flux increasing with decreasing frequencies. Self-absorption of synchrotron radiation from a power-law electron energy distribution leads to an optically thick spectrum in the form of $\nu^{2.5}$. Such expanding plasmoids have been resolved in some X-ray binaries (e.g. Ogley et al. 2001).

A VLBI observation of AE Aqr at 3.6 cm on 1988 January 28–29 showed indeed the radio source which evolved in 30 min from an unresolved source of radius $<0.8a$ (flare peak of 24 mJy) to a resolved source (8 mJy) of radius $\sim 2.5a$ (Niell, private communication). This shows that the brightness temperature evolved from $T_{\rm b} > 1.5 \times 10^{10}$ K down to 5.7×10^8 K: since this latter value is below the range of values adopted by BDC ($10^9 < T_{\rm b}({\rm K}) < 10^{12}$), it shows that synchrotron radiation from electrons of ("final") energies $1 < \gamma \leq 3$, called gyro-synchrotron, also contributes in radio, unless the measured final radio source size is actually composed of smaller, unresolved sources.

Flares were subsequently observed in the millimetre (Abada-Simon et al. 1993; Altenhoff et al. 1994) and they are suspected to be present also in the sub-millimetre since, at 0.761 mm on 1993 October 18, the flux value was 67% larger than on the next day: this suggested that the turnover frequency of the synchrotron spectrum may be ≥394 GHz (0.761 mm) (Abada-Simon et al. 1995b), but with the usual assumption that the source radius is $\leq a/2$, we infer that $10^7 \leq T_{\rm b} < 10^9$ K for both the submillimetre and the millimetre emissions (see Table 2).

On the other hand, the discovery of sudden dips at 2 and 3.6 cm in 10 s resolution data on 1988 June 2–3, which were attributed to eclipses of the radio source via free-free absorption by the accreting gas blobs, implied a much smaller radius ($0.002a$–$0.1a$), which led to brightness temperatures $T_{\rm b} \geq 9 \times 10^{11}$ K (Abada-Simon et al. 1995a). Therefore, the synchrotron emission is from electrons of $\gamma \simeq 200$, and, since Inverse Compton scattering by relativistic electrons limits $T_{\rm b}$ to $\leq 10^{12}$ K for synchrotron sources (Melrose 1994), for $T_{\rm b} > 10^{12}$ K, the emission may therefore be coherent, via a loss-cone instability which can lead to cyclotron or synchrotron maser (Abada-Simon et al. 1996).

In summary, the various data obtained since 1987 at 3.6 cm suggest a radio source radius ranging from $0.002a$ to $2.5a$.

Finally, simulations showed that magnetic pumping is a possible mechanism for the acceleration of particles responsible for both quiescent and flaring radio emissions (Kuijpers et al. 1997). The scenario which can be drawn for the radio emissions of AE Aqr is the following. Part of the material accreted through the L1 point is probably trapped by the white dwarf magnetic field lines. The magnetic pumping process in the white dwarf magnetosphere, driven periodically (at $P_{\rm orb}$) by the relative motion with both the secondary star and the infalling gas, accelerates the electrons sufficiently for them to radiate synchrotron radiation in radio quiescence. However, when the total energy content of the particles becomes comparable to that of the trapping field structure, an MHD instability sets in: presumably *one or several* plasmoids are expelled and cause the observed radio flares (Kuijpers et al. 1997).

1.4. Remaining questions

ISO provided a unique opportunity to measure and possibly link with each other the various contributions of AE Aqr in the unexplored domain ranging from 3.6 to 761 μm. The aim of our ISO near infrared observations was to measure the secondary photospheric emission and other possible contributions from the binary at $\lambda > 3.6$ μm: *i)* the accretion flow; *ii)* cyclotron features at harmonics of the cyclotron frequency $\nu_{\rm c}({\rm Hz}) = eB/(2\pi mc) \simeq 2.8 \times 10^6 B({\rm G})$, in order to determine more accurately the white dwarf magnetic field strength, on which an uncertainty of 3 orders of magnitude remains – an

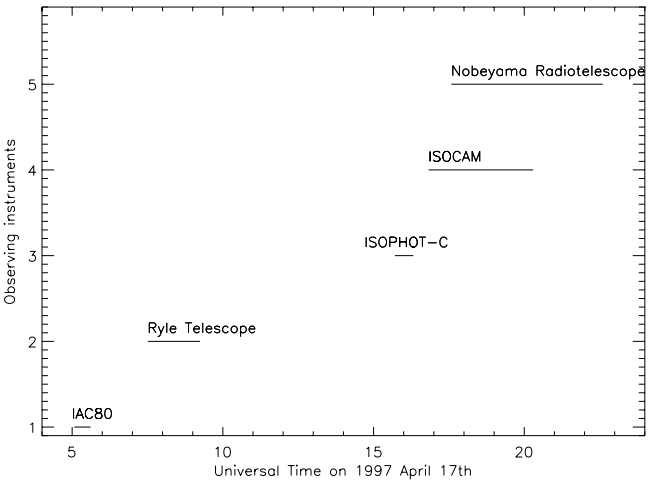

Fig. 1. Scheme of each instrument coverage during the 1997 April 17 multi-wavelength observing campaign of AE Aqr. The *X*-axis is in UT.

accurate field strength is crucial in parameterising the radio-to-infrared emission (a field of 10^7 G should lead to emission on the first harmonic of a cyclotron frequency of value corresponding to ∼6 μm); *iii)* dust; and *iv)* circumbinary disc. These two latter contributions may extend to the far infrared. The far infrared ISO observations and the reprocessed IRAS data also aimed at investigating the extension to the high frequency part of AE Aqr radio spectrum, more particularly to measure the optically thin part of the synchrotron emission. Indeed, there is a number of plasmoid parameters in the radio-to-infrared which are unknown, including: the electron energy distribution function (and its spectral index $-\delta$ if it is a power-law); the electron number density written $n_{\rm e}$ and the magnetic field strength (respectively in cm^{-3} and in Gauss in all this paper); the location, size and expansion velocity; and the evolution with time of the plasmoid parameters. Whereas the optically thick part of an individual plasmoid synchrotron spectrum cannot be measured because the observed radio to far infrared spectrum is due to the superposition of the optically thick and thin synchrotron spectra of all the plasmoids, the optically thin spectrum of the plasmoid, which has the highest turnover frequency is measurable and leads directly to δ.

This paper presents several flux measurements and upper limits for AE Aqr in the near to the far infrared from reprocessed IRAS data (initially recorded in 1983), ISO data obtained on 1996 April 17, and the results of a multi-wavelength coordinated campaign performed contemporaneously with several ISO observations of AE Aqr (see in Fig. 1 the coverage of each instrument in Universal Time on 1997 April 17), in order to give a global view of AE Aqr emissions: our aim was to observe AE Aqr from optical to radio strictly simultaneously with ISO in order to get a unique instantaneous spectrum of the binary covering both the whole synchrotron emission, the secondary spectrum and the other contributions; we also wanted to study possible flux variations with time and their correlations between radio, infrared and optical domains. Unfortunately, all our data could not be recorded simultaneously, but those of 1997 April 17 were obtained within 18 h. In Sect. 2, we present the observations and data reduction; in Sect. 3, we present the observational results and analysis, in Sect. 4, their interpretation, and in Sect. 5, we summarise our results and conclude. The observations of AE Aqr with ISOPHOT-C were initially reported in Abada-Simon et al. (1998); in this paper, we present these data reprocessed.

2. Observations and data reduction

Table 1 summarises the details on all the observations mentioned in this paper: in Col. 1, the date, in Cols. 2 and 3, the start and end Universal Time, in Col. 4, the instrument, in Cols. 5 and 6, the wavelength and corresponding frequency (in GHz), and in Col. 7 the measured average flux density and the 1σ error bar (in mJy).

2.1. Infrared observations with ISO and IRAS

2.1.1. ISO observations

The European Space Agency (ESA) Infrared Space Observatory (ISO) is a satellite that was operational between November 1995 and May 1998 (Kessler et al. 1996). It operated at wavelengths from 2.5 to 240 μm. The satellite essentially consisted of a telescope with a 60-cm diameter primary mirror, and four scientific instruments, among which we used: the Infrared Camera (ISOCAM, see Cesarsky et al. 1996), covering the 2.5−17 μm band with two different detectors, and the photo-polarimeter (ISOPHOT, see Lemke et al. 1996), operating between 2.5 and 240 μm.

AE Aqr was firstly observed with the ISOPHOT photopolarimeter (ISOPHOT-P in the following) on 1996 April 17 in the 4.8 and 7.3 μm filters, using the 7.6 and 10 arcsec diameter apertures, respectively. In the ISO Archive this observation corresponds to a Target Dedicated Time (TDT) number of 15202006; integration times were 256 and 128 s at 4.8 and 7.3 μm, respectively, with half of the time on-source. The PHT chopper was used in triangular mode, with a throw of 90 arcsec between each of the three sky positions. Due to the faintness of AE Aqr and the observing mode, we deviated from the standard processing and derived a special empirical flux calibration based on archival ISOPHOT calibration observations. The data were processed with the ISOPHOT Interactive Analysis (PIA) software package (Gabriel et al. 1997) to Signal per Ramp Data (SRD) level. All measurements were taken with apertures smaller than 23 arcsec, where the appropriate correction factors are not well known (Schulz et al. 2002), and also a strong hook-shaped transient was present, so that the Fine Calibration Source measurement could not be used to perform an accurate flux calibration. However, the relative correction factors for the losses of a celestial point source at the centre of a non-standard aperture are known to follow the theory well (Müller 2000). Fortunately the Si:Ga material of the P1 detector kept a fairly stable responsivity compared to Ge:Ga, so we used the default responsivity of $R = 1.12$ A W^{-1} for the flux calibration, and accounted for filter-to-filter corrections and Point Spread Function (PSF) according to Schulz et al. (2002). We determined the reproducibility of the background subtracted detector signals from 32 observations of the faint

Table 1. Summary of AE Aqr observations in 1983, on 1996 April 17, and from 1997 April 17 to 1997 May 6. ISOPHOT-C200 time is divided into: 15:21:24−15:42:46 (simultaneous with ISOPHOT-C100) and 15:43:28−16:19:04. Nobeyama time at 1.4 cm is divided into: 17:35−18:30 and 20:23−20:53. Nobeyama time at 7.0 and 3.5 mm is divided into: 19:27−20:09, 21:02−21:44 and 21:54−22:36.

(1) Date	(2) Start	(3) End (UT)	(4) Instrument	(5) Wavelength	(6) Frequency (GHz)	(7) Flux $\pm 1\sigma$(mJy) or 3σ upper limit
1983			IRAS	12 and 25 μm	25 000 and 12 000	<99 and <87
1983			IRAS	60 and100 μm	5000 and 3000	90 ± 30 and <237
96/4/17	15:40:48	16:05:40	ISOPHOT-P	4.8 and 7.3 μm	6.2×10^4 and 4.1×10^4	<42.6 and 27.4 ± 6.0
97/3/20	10:30:43	11:24:00	Ryle	2.0 cm	15	3.4
97/3/21	6:23:24	9:15:50	Ryle	2.0 cm	15	5.7
97/3/29	6:46:5	8:41:17	Ryle	2.0 cm	15	8.0
97/4/15	4:49:26	6:24:29	Ryle	2.0 cm	15	2.0
97/4/16	7:35:2	9:18:43	Ryle	2.0 cm	15	6.4
97/4/17	5:14:12	5:36:36	IAC80	0.44, 0.55 and 0.70 μm	(6.8, 5.4 and 4.3) $\times 10^5$	15.0 ± 0.4, 66.7 ± 1.7 and 75.6 ± 1.5
97/4/17	7:30:43	9:14:24	Ryle	2.0 cm	15	2.8 ± 0.5
97/4/17	15:21:24	15:42:46	ISOPHOT-C100	90 μm	3333	113 ± 21
97/4/17	15:21:24	16:19:04	ISOPHOT-C200	170 μm	1765	<108
97/4/17	16:49:42	20:17:30	ISOCAM04	5–7 μm	5.0×10^4	50–20 (±1.4)
97/4/17	17:35	20:53	Nobeyama	1.4 cm	21	<7.4
97/4/17	19:27	22:36	Nobeyama	7.0 and 3.5 mm	43 and 86	<13.5 and <19
97/4/18	7:26:24	9:10:48	Ryle	2.0 cm	15	5.4 ± 0.5
97/5/6	3:7:12	7:53:46	Ryle	2.0 cm	15	5.9 ± 0.6
97/5/6	00:40:39	11:09:29	MERLIN	18 cm	1.658	2.5 ± 0.5

Table 2. Brightness temperatures obtained for the average flux densities measured from radio to infrared, for an assumed source radius of $0.5a$ (same references as those of Fig. 4).

(1) Wavelength	(2) Frequency (GHz)	(3) Average Flux Density (mJy)	(4) T_b (K) for $r = 0.5a$
60 μm	5000	90	4.3×10^5
90 μm	3333	113	1.2×10^6
170 μm	1765	(<108)	($<4.3 \times 10^6$)
761 μm	394	85.8	6.7×10^7
3.4 mm	88	19.6	3.0×10^8
1.3 cm	22.5	14.6	3.2×10^9
2 cm	15	8.0	4.2×10^9
3.6 cm	8.4	7.6	1.3×10^{10}
21 cm	1.4	4.4	2.7×10^{11}

calibration standard HD 172323 at 12 μm. The standard deviation suggests that the P1 absolute flux scale is accurate to about 40% when using default responsivities at small fluxes.

AE Aqr was observed one year later, on 1997 April 17, with ISOPHOT in Camera modes C100 (9 pixels) and C200 (4 pixels) respectively at 90 μm and 170 μm. This observation was divided into the two TDT numbers 51801601 and 51801602; it will be referred to as "ISOPHOT-C" in the following. The on-source integration times were 118 s and 1471 s respectively at 90 μm and 170 μm. PHT chopped measurements require solutions for the 3 following issues: *i)* there are too few integration ramps (mostly 2*4) in one chopper cycle to give good enough statistics, to reliably detect glitches and spontaneous spiking. *ii)* The long time constants of the detector response lead to an underestimation of the signal difference between the two chopper positions. *iii)* The flux received at the detector is a function of the chopper deflection angle, so a signal difference between two chopper positions does not necessarily mean that the flux at both positions is different. This zero point is not very well known and confusion at longer wavelengths complicates the assessment further. *i)* A larger amount of datapoints and thus more reliable statistics with respect to glitches was obtained by

subdividing each integration ramp – that in our case had 32 to 64 readouts – into subramps of 4 to 8 readouts. The total useful integration time increased too since outliers from high energy radiation hits waste less integration time when removed. Ramp subdivision is a standard method available in PIA, which has been successfully used on other ISOPHOT data (i.e. Clavel et al. 2000). In addition the baseline drift of the detector signal was removed, since it can – in extreme cases – lead to significant systematic changes of the difference between on and off position. The baseline was calculated by a boxcar smoothing function with high time constant (120 s). All PIA standard corrections were applied as well: ramp linearity, reset interval correction, dark subtraction, vignetting correction and signal linearization.

ii) Underestimation of flux in chopped observations of very weak sources due to transients are found to have a significant impact only on the C100 detector (90 μm observation). We corrected for this by reducing archival observations of known sources of comparable brightness and similar instrument setup in the same way as the ones of AE Aqr. We make use of the fact that under similar conditions the detector transients behave comparably. The comparison of the derived result and the known value for the calibrator delivers a calibration correction factor. The first calibrator was SAO248381 (TDT 25000801), which showed the same instrument configuration, except that the integration time was only 256 s. The reduction to Signal per Chopper Plateau level gave a PSF corrected inband power of $5.25 \times 10^{-17} \pm 1.73 \times 10^{-17}$ W. The expected inband power (see Schulz et al. 2002) is 1.558×10^{-16} W, yielding a correction factor of 2.97. Since the detection is only marginal, a second observation of a calibrator (HR 7310, TDT 84602004) was selected. The different filter (100 μm) is not expected to affect the correction factor. The raw result there was $5.657 \times 10^{-17} \pm 1.089 \times 10^{-17}$ W (before PSF correction), while 2.167×10^{-16} W were expected, giving a correction of 2.18. From these results we adopt a correction factor of 2.6 and a flux uncertainty of 30% for sources of similar brightness observed with C100 using the described reduction method.

iii) The third issue turned out to affect the 170 μm measurements (C200 detector). Both measurements show the same pattern in the four pixels, but the errors are clearly smaller than the differences between right and left chopper position and are sometimes negative with a signal-to-noise ratio better than 3. In order to estimate the arising systematic uncertainties, a measurement with the same instrumental setup was found in the archive, which was most likely a non-detection too (TDT 10102302 on HR 6180 which is a K2III star with a 25 μm IRAS flux of 0.58 Jy and only upper limits at 60 and 100 μm). Again the data reduction gave significant negative and positive values, delivering a systematic uncertainty which we attribute to both the sky confusion and uncertainties in the zero point (chopper vignetting).

Also on 1997 April 17, AE Aqr was observed using ISOCAM (TDT 51801603). The Long Wavelength camera was used in CAM04 mode. In this mode Circular Variable Filters were stepped in wavelength so that a spectrum can be created. In this observation the wavelength range covered was 4.956−6.968 μm. The ISOCAM suite of software CIA v4.0 was used to analyse the data. AE Aqr was detected at all wavelengths at a significant level. A background subtracted spectrum was created by extracting a spectrum from the source and a spectrum from a much larger area of sky background. A background subtracted spectrum was then made by suitably scaling the areas used in each extraction.

2.1.2. IRAS observations

The IRAS (Beichman et al. 1988) data were obtained in 1983, between January and November. The IRAS pointing accuracy was ∼30 arcsec. We used the IRSA (Infra-Red Science Archive) analysis tool SCANPI V5.0[3] to process the IRAS individual scans specifically at the AE Aqr position. No other source was found within a radius of 10′. We changed a few processing parameters with respect to the defaults. The data ranges for 12 μm and 25 μm were set to 8′ and 16′ respectively. The polynomial to fit the baseline was set to degree 3 and the most noisy scans were manually deselected.

SCANPI offers four different ways of combining the scans that crossed the region of interest: *i)* the weighted mean with weights of 1 or 0.5 (for a few noisy detectors); *ii)* the straight mean; *iii)* the statistical median; *iv)* the noise-weighted mean. Although the online documentation gives some guidance, it does not identify a definite procedure on how to derive a final solution for photometry. We based our selection of results on the consistency of the results for all combination methods and scan graphs provided by the software. It appears that the weighting method using values of 1.0 and 0.5 seems to be the least reliable to provide good flux calibration, while the median method seems to be the least reliable to provide good uncertainties. We selected those results that were most consistent in methods *ii)*, *iii)* and *iv)*.

We verified our procedure by processing the closest IRAS source F20384-0103 that is within 15′ of AE Aqr. The result is consistent with the IRAS Faint Source Catalog (FSC) entry and improves the 100 μm value for F20384-0103 to be a detection of 360 ± 93 mJy within the upper limit of the IRAS FSC of 701 mJy, which is labeled as detected only at 60 μm with 261 mJy.

2.2. Optical observations

Photometric observations of AE Aqr in the Johnson *B*, *V* and *R* bands were performed on the night of 1997 April 16−17, with a Thomson CCD camera at the Cassegrain focus of the 80 cm telescope IAC80 at the Izaña observatory (Tenerife, Spain). We used integration times of 60 s (*B*), 45 s (*V*) and 30 s (*R*) which resulted in 360 s time resolution for each filter. The images were de-biased and flat-fielded in the standard way using

[3] This research has made use of the NASA/IPAC Infrared Science Archive, which is operated by JPL, California Institute of Technology, under contract with NASA.

IRAF[4]. We performed relative PSF photometry (Stetson 1987) of AE Aqr with respect to several comparison stars in the field. These were flux calibrated on the night of 7 October 2001 by observing the nearby comparison BD-014021 (see van Paradijs et al. 1989), only 9 arcmin to the East of AE Aqr, and the flux standard Landolt 112−275 under photometric conditions.

2.3. Radio observations

Centimetric-millimetric observations of AE Aqr were performed with the 45 m Radio Telescope of Nobeyama (Japan) on 1997 April 17, alternately at 21.0 GHz (1.4 cm) and at both 43.0 and 86.0 GHz (resp. 7.0 cm and 3.5 mm) simultaneously. The HEMT receiver was used at 21 GHz, and the SIS receiver at 43 and 86 GHz. The observing conditions were a temporal strong wind (3−10 m/s) and heavily clouded. The primary calibrator used was NGC 7027, which flux density values are 5.90 Jy at 21 GHz, 5.45 Jy at 43 GHz, and 5.3 Jy at 86 GHz (Ulich 1981). The pointing and flux references used were 2059+034 (2.66 Jy at 21 GHz), 2134+004 (3.0 Jy at 43 GHz and 1.7 Jy at 86 GHz), which are assumed not to vary within the observation.

AE Aqr was also observed in a series of short observations (typically 1−2 h) at 15 GHz (2.0 cm) with the Ryle Telescope (Cambridge, UK), between 1997 March 20 and April 18, including the 17. The Ryle Telescope is a synthesis telescope operating at 15 GHz, and only 5 antennas were used in this particular observation. A 5-h observation was also performed on 1997 May 6, simultaneous with the MERLIN observation described below. In each case, the observations followed the pattern described by Pooley & Fender (1997), using (in this case) the nearby source J2050+0407 as a phase calibrator. The original sampling interval was 32 s.

Observations with the Multi-Element Radio Linked Interferometer Network (MERLIN) were also performed on 1997 May 6 at 1.658 GHz (18.1 cm). MERLIN, operated by Jodrell Bank Observatory, is an array of radio telescopes distributed around UK, with separations of up to 217 km. The largest antenna has a 76-m diameter, the second largest is 32-m, and three others measure 25-m. The spatial resolution is around 0.2 arcsec. A standard MERLIN setup was used at 1.658 GHz, with a 14 MHz total bandwidth in Left and Right Circular polarizations. The flux calibration relative to 3C 286 (13.64 Jy) using OQ208, was found to be 1.15 Jy. The phase calibrator was 2039+037, found to be 117 mJy and unresolved. The data were averaged for 20 min. using 3 of the most sensitive baselines. The 1σ error per point is ∼3 mJy.

3. Observational results and analysis

3.1. Infrared and optical results

Figure 2 shows the average flux densities and upper limits of AE Aqr measured in 1983 (reprocessed IRAS data), and from 1996 April 17 to 1997 May 6 between 18 cm and 0.44 μm. The details on these results are reported in Table 1. In optical, AE Aqr was in a quiescent phase with a flux at the known lowest levels, and it was very stable, with a variability of ≤5 mJy.

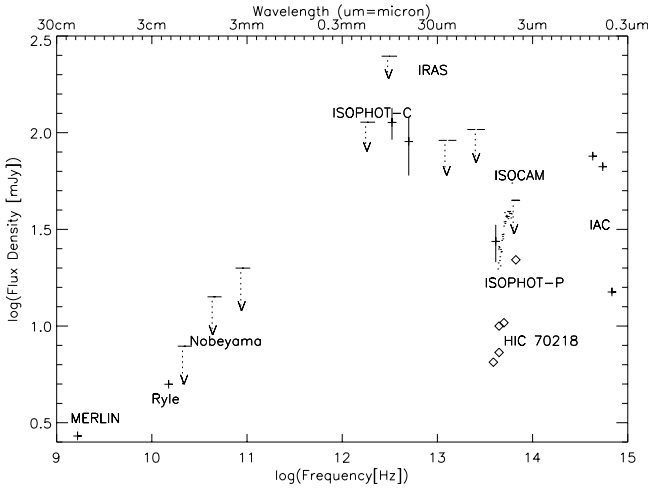

Fig. 2. Average flux densities (in mJy; represented by "+" symbols) of AE Aqr and their 1σ error bar versus increasing frequency (in Hz) on the lower axis, and versus decreasing wavelength on the upper axis, as measured between 18 cm and 0.44 μm: by IRAS at 12, 25, 60 and 100 μm (recorded in 1983, but reprocessed for this paper); between 1996 April 17 and 1997 May 6: by MERLIN at 1.658 GHz, the Ryle telescope at 15 GHz (only the average 5.0 mJy of the eight days is plotted), the Nobeyama telescope at 21.0, 43.0 and 86.0 GHz, ISOPHOT-C at 90 and 170 μm, ISOPHOT-P at 4.8 and 7.3 μm, and IAC80 at 0.44, 0.55 and 0.70 μm. The 3σ upper limits are marked by a dotted vertical arrow starting from a horizontal dash. The ISOCAM spectrum (from ∼7.0 to 5.0 μm) measured on 1997 April 17 is represented by the 35 dots; the isolated dot at 4.956 μm just below the label "ISOCAM" is real. The diamonds are the fluxes of the comparison K5V star HIC70218 measured with ISO between 5 and 8.5 μm, and averaged over various wavelength bands.

With ISOPHOT-C, AE Aqr was detected at 90 μm with a mean flux of 113 mJy at the 5.4σ level; at 170 μm, the 3σ upper limit was 108 mJy. Note that all flux densities are not color corrected, and that the C160 fluxes are not PSF corrected. In addition, the signal-to-noise ratio was too low to measure any flux variation with time.

With IRAS, the scan plots suggest a source detection of 50 and 55 mJy respectively at 12 and 25 μm for AE Aqr, however the formal S/N values are only 1.5 and 1.9 respectively. The final results for AE Aqr with IRAS are then: 3σ upper limits of 99, 87 and 237 mJy respectively at 12, 25 and 100 μm; AE Aqr was detected at the flux level of 90 ± 30 mJy (3σ) at 60 μm.

If the 60 and 90 μm emissions are of the same origin, then their relative bandwidth is $\Delta f/f \simeq 0.4$ (40%). For both our ISO and IRAS data, there is no information on the polarization, and no time variability measurement.

With ISOPHOT-P, assuming a source color equivalent to a blackbody of 6000 K, correction factors of 1.12 and 1.07 were applied for the 7.3 and 4.8 μm filters respectively. Finally the instrument specific signals translate into 27.4 ± 6.0 mJy at 7.3 μm and 40.0 ± 14.2 mJy at 4.8 μm. The uncertainties are

[4] IRAF is distributed by the USA National Optical Astronomy Observatories, which is operated by the Association of Universities for Research in Astronomy, Inc., under contract with the USA National Science Foundation routines.

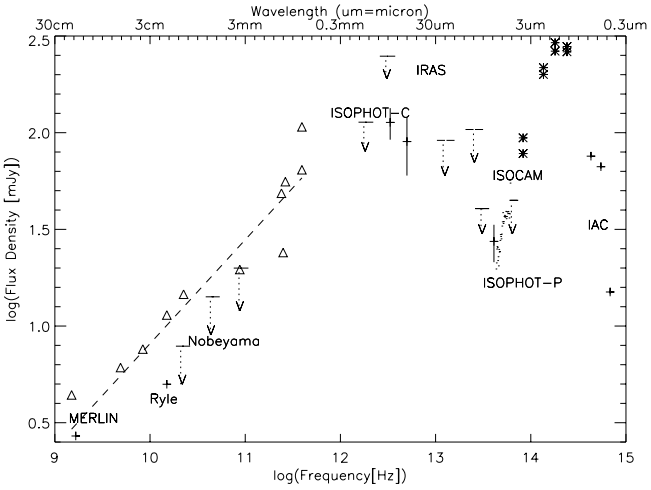

Fig. 3. Same as Fig. 2, but only for AE Aqr (i.e. without the comparison star), and with, in addition, average radio-to-near-infrared data since 1981. The stars in the upper right part of the figure represent the flux density values measured in the *J*, *H*, *K* and *L* bands by Tanzi et al. (1981). The 3σ upper limit of 40.5 mJy at 10 μm is also plotted (from BSC85).The triangles in the left-hand part part of the figure represent the average fluxes of AE Aqr from 22 cm to 0.761 mm measured between 1988 and 1993, and reported in the literature (a fit of the 14 average fluxes between 22 cm and 0.761 mm gives an average index of +0.5 and is represented by the dashed line); they were obtained using the VLA at 1-to-21 cm between 1984 and 1993, the IRAM-Plateau-de-Bure-Interferometer at 3.4 mm in 1991, both the IRAM-30-m telescope and the Caltech Submillimetre Observatory at 250 GHz (1.2 mm) in 1990, and the JCMT at 0.761 and 1.1 mm in 1993 (references: BDC; Abada-Simon et al. 1993; Altenhoff et al. 1994; Abada-Simon et al. 1995a,b).

statistical and make the 7.3 μm observation a 4.6σ detection and the 4.8 μm measurement a 3σ upper limit of 42.6 mJy.

The ISOCAM spectrum increases from ~20 mJy at ~7.0 μm to ~50 mJy at ~5.0 μm (average rms: 1.4 mJy only). The low signal-to-noise prevented us from splitting into different spin phases. Further, the mean spectrum shows no obvious sign of cyclotron features.

At 7.3 μm, ISOPHOT-P has then measured a flux slightly higher than at ~7.0 μm (ISOCAM), but with an uncertainty larger than that on ISOCAM data, which suggests a common origin for the two emissions.

To summarise, this is the first time that AE Aqr has been detected from 5 to 90 μm, and that constraining upper limits have been obtained between 12 and 170 μm.

The detections at 90 and 60 μm can be fitted by a line of slope ~−0.6 on the log-log plot (Fig. 3) and they are in agreement with the plotted upper limits from 100 to 10 μm; the IRAS upper limit at 12 μm shows that the spectrum cannot be substantially less steep between 90 and 12 μm.

3.2. Radio results

In Nobeyama, the data were acquired during bad weather and with a limited stability of the data. At 1.4 cm, we derived an average flux of 6.7 ± 2.5 mJy (1σ), which makes it a 3σ upper limit of 7.5 mJy; however, because the 1.4 cm measurement is based on cross scan over the source, positional coincidence of the positive signal supports a detection. At 7.0 cm and 3.5 mm, the 3σ upper limits are 13.5 mJy and 19 mJy respectively. Since AE Aqr has been detected several times at ~1.4 cm (with the VLA) and at 3.4 mm (with the IRAM Interferometer) at flux levels both lower and higher than these Nobeyama upper limits, the non-detections can be explained by both bad weather and the probably non flaring state of the source.

At 2.0 cm (Ryle Telescope), AE Aqr was faint but variable, ranging from 1 or 2 mJy to ~14 mJy on 1997 May 6. For comparison, some data from 1988 to 1996 show means of 8.0−11.4 mJy, respectively, and some excursions to 20 mJy, so the observations of Spring 1997 show a lower flux than usual at the same frequency. There is clear evidence that the source varies by factors up to ≥10 on timescales of the order of 30 min.

AE Aqr was observed on 1997 May 6, at 18.1 cm, using MERLIN. The radio map shows a point source from which we can determine a position accurate to at least 100 milliarcsec (mas). There is a very weak extension as well as a nearby (about 1/2 arcsec) source at about the 0.4 mJy level, although it is not certain if this was just a random noise fluctuation. The Very Large Array (VLA) archive shows a very large amount of observations of this source, in many configurations and frequencies, the best of which would have had comparable resolution to these MERLIN observations. Fitting of a Gaussian to best map of AE Aqr gives a FWHM of 200 mas, with a total flux density of 2.5 mJy. So there is no significant emission (i.e. more than 3σ = 0.3 mJy) at a distance larger than 100 mas from the core.

4. Interpretation and discussion

4.1. First implications from the infrared measurements

The K5V single star HIC 70218 was observed using ISO in the same setup as the ISOCAM observations of AE Aqr. The flux values of this comparison star, measured in various filters between 4 and 8.5 μm, and placed at AE Aqr distance are plotted as diamonds in Fig. 2. Assuming that these values represent the spectrum of AE Aqr K5V secondary, and since they are ~10−20 mJy below the fluxes measured for AE Aqr by ISOCAM between ~5.0 and ~7.0 μm and by ISOPHOT-P at 7.3 μm, it suggests that thermal emission from the accretion stream and some possible weak cyclotron emission from the post-shock accretion material close to the white dwarf add a substantial contribution to that of the secondary spectrum. Like in other CVs near infrared light, it is difficult to distinguish the proportion of flux which comes from these two components with respect to that of the red dwarf secondary.

Another contribution to these ISO emissions could be thermal emission from dust grains, as expected by BSC85 at 10 μm (3σ upper limit of 40.5 mJy). The detection at 90 μm with ISOPHOT-C gives an upper limit on the dust mass: if (for example) the 90 μm point is the peak of the dust emission then the dust temperature is ~43 K and the dust mass is $2.9 \times 10^{-8}\ M_{\odot}$ (using the Planck mean emissivity for silicate grains of size 0.1 μm from BSC85). In addition, if a large fraction of the emission at 90 μm is synchrotron, then this is a strong upper

limit. On the other hand, BSC85 speculated that any grains formed must have done so in a "prehistoric nova explosion", but this is unlikely as there is no reason why any nova dust should remain in the vicinity of the system. In addition, the magnetic propeller model of WKH97 indicates that most of the material is expelled from the system, so that the mass-loss rate ($\sim 1-5 \times 10^{17}$ g/s) is far too low to give a high enough density for grains to form. All this points to there being no dust in the environment of AE Aqr as in the majority of other CV systems.

Figure 3 shows that both the ISOPHOT-C 90 μm and IRAS 60 μm detections, the ISOPHOT-C 170 μm upper limit, and the older JCMT 761 μm average flux (Abada-Simon et al. 1995b) are of the same order of magnitude. The two ISOPHOT-C measurements are in agreement with, but more constraining than the IRAS upper limit at 100 μm. Our detections suggest that the flux of AE Aqr decreases from $\lambda \leq 90$ μm down to ~ 7 μm: this is consistent with the upper limits of IRAS at 25 and 12 μm and of BSC85 at 10 μm. Below we review the mechanisms which could account for our new results obtained between 4 and 170 μm. We recall that the IRAS data were obtained in 1983 and the ISO data in 1996−1997, so that all what follows treats an "average" spectrum spanning over 15 years, whereas it is observed in radio that the flux exhibits changes of a factor ≥ 2 in about 10 s.

Firstly, in order to fit the flux measured at both 90 and 60 μm using a blackbody, it needs to be a temperature of $\sim$56 K, but with a radius of $\sim 158a$, which is huge. However, we notice that it is of the order of the maximum radius of the Circum-Binary (CB) discs predicted by DTS at 100 μm in CVs: they are modelled using several blackbodies of temperatures between 30 and 3000 K; DTS predicts that it leads to a flux density $\propto \nu^{0.6}$ in the infrared, with $\sim$300 mJy at 10 μm (for a CV at 100 pc). The value of 20 mJy measured by ISOCAM at 7 μm implies that, if there is any CB disc in AE Aqr, its temperature T and radius r are such that, assuming a single blackbody (to simplify the following estimates), then the term $\frac{r^2}{e^{h\nu/kT}-1}$ is a factor 15 smaller than predicted by DTS (see Fig. 4). This could be possible if the temperature of the CB disc and/or its radius were smaller, and since the secondary temperature in AE Aqr is higher than the one assumed by DTS, the CB disc could be even smaller with a temperature which could be higher. Finally, the mid infrared flares of Dubus et al. (2004) are more compatible with our far-to-mid infrared data than with a CB disc.

In order to estimate whether the emission process is thermal or not, let us firstly estimate the brightness temperature corresponding to the fluxes measured $\lambda \geq 60$ μm. We have seen in Sect. 1.3 that, assuming isotropic emission from a spherical source, at wavelengths $\geq$60 μm, the brightness temperature is given by Eq. (1): let us assume that the source diameter is not larger than the binary separation, that is, its radius is $r \leq a/2$, then at 90 μm we find $T_\mathrm{b} \geq 1.2 \times 10^6$ K and at 60 μm, $T_\mathrm{b} \geq 4.3 \times 10^5$ K. If these fluxes correspond to the same source of emission, then the bandwidth of this emission is rather large ($\Delta f/f \simeq 0.4$); there is no information on any time variability nor on the degrees of polarization. Therefore, the obtained values of T_b lead us to consider whether thermal bremsstrahlung (or "free-free radiation") is possible or not at 60 and 90 μm. This mechanism is invoked for T_b up

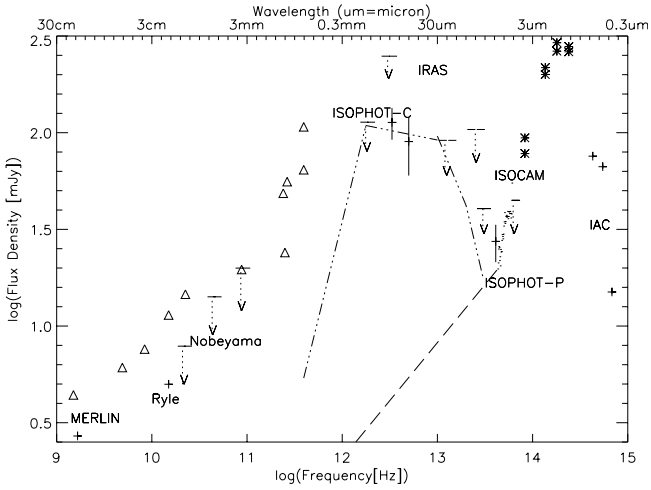

Fig. 4. Same as Fig. 3, with, in addition: the highest possible emission from a Circum-Binary disc, if any (large dashed line of index 0.6); the three parts of a thermal bremsstrahlung spectrum fitting the far-to-mid infrared data (dash-triple dot lines: of indices 2 and −0.1, and then of exponential decrease).

to $\sim 10^7$ K, whereas "gyro-synchrotron" radiation from a thermal distribution of electrons or from a non-thermal energy distribution of mildly relativistic electrons (up to a few MeV, that is $1 < \gamma < 10$) must lead to $10^7 \leq T_\mathrm{b} \leq 10^9$ K, and "synchrotron" radiation from a non-thermal distribution of ultra-relativistic electrons ($\gamma \gg 1$) must lead to $10^9 \leq T_\mathrm{b} \leq 10^{12}$ K (e.g. in solar emissions, Dulk 1985; Melrose 1994). Dulk (1985) underlines that, free-free emission varying as $n_\mathrm{e}^2 T^{-1/2}$, it dominates over gyrosynchrotron (varying as $n_\mathrm{e} T^\alpha B^\beta$) if the electron number density n_e is high enough, or if either the temperature T or the magnetic field strength B are low enough. In the following sections, we will envisage bremsstrahlung and "magneto-bremsstrahlung" (this term holds for both gyro-synchrotron and synchrotron). For the flux densities measured at various epochs from the mid-infrared to the radio domains, Table 2 shows the wide range of T_b obtained for an assumed source radius of $0.5a$; we then see that:

- Thermal bremsstrahlung may dominate at $\lambda \leq 170$ μm for $r \geq 0.5a$ since $T_\mathrm{b} < 10^7$ K.
- Magneto-bremsstrahlung may dominate with the following characteristics (see also Table 3):
  * $10^7 \leq T_\mathrm{b} \leq 10^9$ K in the millimetre-submillimetre ranges for $r \simeq 0.5a$ and at shorter wavelengths for smaller radii,
    and/or
  * $T_\mathrm{b} \geq 10^9$ in the centimetre-decimetre ranges for $r = 0.5a$ and at shorter wavelengths for smaller radii.

4.2. Thermal Bremsstrahlung in the mid-to-far infrared?

Let us estimate under which conditions thermal bremsstrahlung can account for the mid to far infrared data. The thermal bremsstrahlung spectrum has three "parts" (Fig. 4). The optically thick part at low frequencies ν below a critical

Table 3. For various wavelengths, values of source radius (in units of the binary separation a) leading to brightness temperatures corresponding to gyro-synchrotron (Col. 2) and synchrotron (Col. 3) – references in Sect. 1.3.

(1) Wavelength	(2) $r[a]$ implying $T_b = 10^7$–10^9 K	(3) $r[a]$ implying $T_b = 10^9$–10^{12} K
90 μm	0.017–0.17	0.0005–0.017
0.761 mm	0.14–1.4	0.005–0.14
3.4 mm	0.44–4.4	0.014–0.44
1.3 cm	1.6–16.0	0.05–1.6
3.6 cm	2.9–29	0.09–2.9
21 cm	13.5–135	0.43–13.5

frequency ν_{LF} (where the optical thickness is $\tau \simeq 1$) follows the Rayleigh-Jeans law of spectral index +2: at the distance of AE Aqr (102 pc), still assuming a spherical source of radius r (in cm) emitting isotropically, it can be written as

$$S_\nu(\mathrm{mJy}) \simeq 10^{-51} T r^2 \nu^2 \quad (2)$$

where T is the average temperature of the thermal distribution of electron energy.

At $\nu > \nu_{LF}$, the optically thin part is firstly dominated by a spectral index of −0.1, which corresponds to an almost flat spectrum on a log-log plot:

$$S_\nu(\mathrm{mJy}) \simeq 7 \times 10^{-52} r^3 T^{-0.5} n_e^2 \nu^{-0.1} \quad (3)$$

where n_e is the electron number density in cm^{-3} (Pacholczyk 1970).

At high frequencies near $\nu_{HE} \simeq kT/h$, the spectrum decays drastically as:

$$S_\nu(\mathrm{mJy}) \simeq 3 \times 10^{-53} r^3 T^{-0.5} n_e^2 g_{ff} e^{-h\nu/kT} \quad (4)$$

where g_{ff} is the Gaunt factor (Rybicki & Lightman 1979).

Figure 4 suggests that a bremsstrahlung spectrum may account for the observed data with: the 60 and 90 μm fluxes on the almost flat part – that is $c/\nu_{LF} > 90$ μm – and the exponential decay at $25 \leq \lambda(\mu\mathrm{m}) < 60$; taking $c/\nu_{HE} \simeq 25$ μm leads to $T \simeq 575$ K. In addition, assuming that the flux at 170 μm is in the optically thick part of the thermal bremsstrahlung (i.e. that $170 \leq c/\nu_{LF} \leq 90$ μm) Eq. (2) implies $r < 8 \times 10^{12}$ cm ($\sim 40a$). Let us take $r = 7 \times 10^{12}$ cm, then the 60 μm flux assumed to be on the flat part implies that the electron number density is $n \simeq 4 \times 10^8$ cm^{-3} (from Eq. (3)). Injecting the values adopted for T, r and n in Eq. (4), we find flux densities increasing from ∼6 to 30 mJy with wavelength from 10 to 30 μm, which are values in agreement with our upper limits. If we took $761\ \mu\mathrm{m} \leq c/\nu_{LF} \leq 170\ \mu$m, then we would get $a/2 \leq r \leq 300a$ for $a\ few\ 10^7 \leq n_e\ (\mathrm{cm}^{-3}) \leq 3 \times 10^{11}$: let us see if this is possible. Since the thermal infrared source is large, then it implies that the radio source would be inside of it, so any density higher than 2.4×10^{10} cm^{-3} around the radio source must be discarded since it would cut the actually measured radio emissions (it corresponds to a plasma frequency above 1.4 GHz ($c/(21\ \mathrm{cm})$)). The column density of matter inferred for $r = 7 \times 10^{12}$ cm and $n \simeq 4 \times 10^8$ cm^{-3} is $N_H \simeq rn \simeq 2.8 \times 10^{21}$ atoms cm^{-2}: a larger value would not be realistic since it would absorb X-rays.

Since the radio to submillimetre average spectrum may apparently be divided into two parts of different slopes with a steepening near 1.2 mm, the optically thick part of the bremsstrahlung could be the steepest part (1.2 mm−761 μm), whereas the less steep part ($\lambda \geq 1.2$ mm) could be magneto-bremsstrahlung. The spectrum of a hybrid thermal-nonthermal plasma has been calculated by Lin & Liang (1999): the non-thermal synchrotron dominates at the lowest energies and the thermal bremsstrahlung at the highest ones.

In summary, the 60 and 90 μm fluxes could be attributed to thermal bremsstrahlung from a source of temperature ≃575 K, of radius $\simeq 7 \times 10^{12}$ cm $\simeq 40a$ and of electron number density $\simeq 4 \times 10^8$ cm^{-3}. Note that the temperature is much below the brightness temperature initially inferred, and that the source radius is much larger than the initially assumed value of $a/2$. Significantly larger or smaller parameters for a thermal bremsstrahlung source in AE Aqr could hardly be compatible with all the observational constraints. It is also hard to imagine a volume of plasma of radius as high as $\sim 40a$, especially because it should be dense enough so that its thermal bremsstrahlung dominates over (gyro)-synchrotron; alternatively, the origin of such a source could be partly the gas which is propelled away from the system, but WKH97 suggest it is rather concentrated in the orbital plane. Any so large source, if it exists, should be resolved by future observations in the infrared.

4.3. Magneto-bremsstrahlung from radio to the infrared

We have just seen that we could hardly account for the observed spectrum at $\lambda \leq 1$ mm with thermal bremsstrahlung; the lower frequency part would remain attributed to synchrotron. We now show why the scenario which is probably the most compatible with the observations is an initially small infrared source composed of several distributions (possibly both thermal, and non-thermal, mildly relativistic electrons) which radiates gyro-synchrotron and expands moderately; it requires to be re-energised (cf. Meintjes & Venter 2003) in order to lead to the observed, larger, radio source of highly relativistic electrons (in the form of several non-thermal distributions) which produce synchrotron.

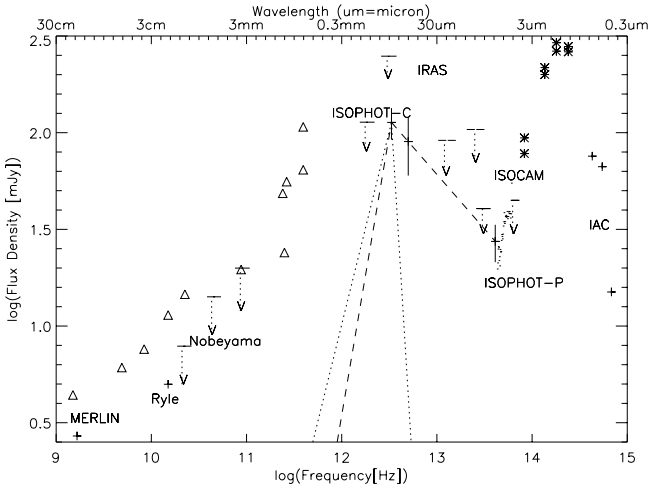

Fig. 5. Same as Fig. 3, with, in addition, the two possible theoretical gyro-synchrotron spectra fitting the far infrared data: that of a thermal electron energy distribution (dotted lines of indices 2 and −8), and that of a power-law distribution (dashed lines of indices 2.9 and the measured value of ≤−0.6).

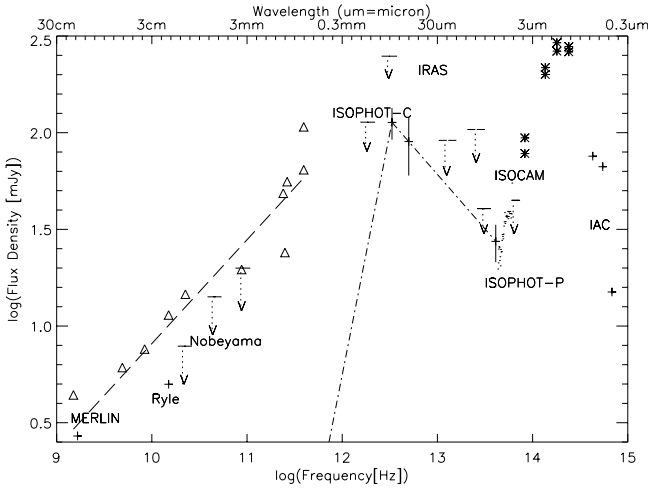

Fig. 6. Same as Fig. 3, with, in addition: the synchrotron spectrum of a power-law distribution fitting the infrared data (dash-dot lines of indices 2.5 and the measured value of ≤−0.6), and the line fitting the radio-to-submillimetre average fluxes (large dashed line of index 0.5).

4.3.1. Gyro-synchrotron radiation from both thermal and non-thermal ($1 < \gamma < 10$) electron energy distributions from the mid infrared to ∼1 mm

Table 3 shows that brightness temperatures of $10^7 \leq T_b \leq 10^9$ K are found for a source of radius $0.017a \leq r \leq 0.17a$ at 90 μm; the same range of T_b is found for source radii larger at longer wavelengths, and in particular for $r \simeq 0.5a$ at $\lambda \simeq 0.761-3.4$ mm. Here, gyro-synchrotron emission from both thermal and non-thermal electron energy distributions seems to be the best explanation for the millimetre-to-mid infrared spectrum for the following reasons.

- The spectrum of gyro-synchrotron from a thermal distribution has an optically thick index of +2 (cf. thermal bremsstrahlung), which fits well the part 0.761 mm $\leq \lambda \leq$ 1.3 mm but an optically thin index of −8 (Dulk 1985): this very steep decrease is not observed, unless it occurs in the two domains which remain unexplored: 90−761 μm and 7.3−60 μm (Fig. 5). Therefore, if there is a thermal gyro-synchrotron contribution, either some process alters its expected spectrum, or its optically thin part is dominated by another source of emission.
- The spectrum of gyro-synchrotron emission from a power-law distribution is a power-law with optically thick and thin indices (resp. 2.9 and $-(0.9\delta - 1.2)$, from Dulk 1985) which are even steeper (for $\delta > 1.75$) than those of the synchrotron from a power-law (resp. 2.5 and $-(\delta-1)/2$): therefore, gyro-synchrotron from one power-law cannot explain the observed optically thick spectrum; if the observed far-mid infrared emission (of index ≤−0.6) is gyro-synchrotron emission from one power-law, then $\delta \geq 2$.

Also, gyro-synchrotron emission is expected to lead to a degree of circular polarization higher than synchrotron does: whereas it has been measured to be <10% in radio, where synchrotron is favored, it requires to be measured at $\lambda < 1$ cm, in order to confirm or infirm the presence of a gyro-synchrotron contribution.

4.3.2. Synchrotron ($\gamma \gg 1$) emission from several non-thermal electron energy distributions at $\lambda \geq 1$ mm

We would need a source radius as small as $0.0005a$–$0.017a$ at 90 μm to find brightness temperatures of $10^9 \leq T_b \leq 10^{12}$ K; note that the largest far infrared radius (∼$0.017a$) is only ∼2 times smaller than the smallest possible radio radius inferred from dips at 2−3.6 cm (Abada-Simon et al. 1995a). The same range of T_b (10^9–10^{12} K) is found for $r \simeq 0.43a$–$13.5a$ at 21 cm, smaller values at shorter wavelengths, and in particular for $r \simeq 0.5a$ at $\lambda \simeq 1.3$–21 cm (cf. Table 3). The synchrotron spectrum from a single power-law electron energy distribution is plotted in Fig. 6: its optically thick part (index +2.5) is steeper than the observed time-averaged spectrum in radio. Synchrotron emission from several non-thermal distributions of highly relativistic electrons ($\gamma \gg 1$) seems to be the best explanation for AE Aqr radio emission ($\lambda \geq 1$ mm).

4.3.3. Implications of the magneto-bremsstrahlung for the source parameters

Assuming that the source is a sphere of angular diameter θ (in arcseconds), the turnover frequency, i.e. where the optical thickness is $\tau \simeq 1$, is:

$$\nu_m(\mathrm{Hz}) = 3.4 \times 10^7 \left(\frac{S_{\nu_m}}{\theta^2}\right)^{2/5} B^{1/5} \quad (5)$$

where S_{ν_m} is the maximum flux density (in Jansky) measured at ν_m, and B is the magnetic field strength in the source (in Gauss in all this paper). Measuring S_{ν_m} at ν_m leads to the corresponding source radius:

$$r_m(\mathrm{cm}) = 3.9 \times 10^{24} \sqrt{S_{\nu_m}} B^{1/4} / {\nu_m}^{5/4}. \quad (6)$$

B cannot be larger than each of the two star surface field strengths: concerning the secondary, it is known that red stars have a photospheric field strength which may be up to ∼1 kG; assuming that the source magnetic field strength cannot exceed the lower limit of the White Dwarf magnetic field, that is $B \leq 10^4$ G, implies $r_{\rm m} = 0.22a$ for $\nu_{\rm m} = 394$ GHz (0.761 mm) hence $T_{\rm b} = 4 \times 10^8$ K, and $r_{\rm m} = 0.02a$ for $\nu_{\rm m} = 3333$ GHz (90 μm) implying $T_{\rm b} = 10^9$ K. Since $r_{\rm m} \propto B^{1/4}$, for a source field of 1 G, the inferred source size would be 10 times smaller; for $B_{\rm WD}$ up to 10^7 G, it would be 5.6 times larger: the initial radius for a plasmoid which synchrotron spectrum firstly peaks at 90 μm would then be $r \leq 0.11a \simeq 20R_{\rm WD}$, which implies $T_{\rm b} \geq 3 \times 10^7$ K. These results are consistent with gyro-synchrotron if the source magnetic field strength is $B \simeq 10^4$–10^7 G; to be consistent with synchrotron ($10^9 \leq T_{\rm b}({\rm K}) \leq 10^{12}$), the source initial field would have to be $B \leq 10^4$ G at 90 μm, and ≤1.6 kG at 0.761 mm. The theory predicts that both $\nu_{\rm m}$ and $S_{\nu_{\rm m}}$ decrease while $r_{\rm m}$ increases with time, so that, in particular, a time delay of the low-frequency flare peaks should be measured with respect to the higher frequency flare peaks. As the 170 μm observation was performed, for one part simultaneously with the 90 μm one, and for the second part immediately after, a simple explanation for the non detection at 170 μm is that the synchrotron spectrum of a plasmoid which peaked at 90 μm (flux 113 mJy) shifted with time to lower (undetected) flux values at lower frequencies.

Several other reasons are invoked to explain why the observed optically thick spectrum can be less steep than the self-absorbed one: we are considering average flux values measured over 15 years, probably from both thermal and non thermal electron energy distributions. A flattening has also been observed in the synchrotron spectrum of X-ray binaries containing a black-hole candidate and of Active Galactic Nuclei, which is explained by a compact jet of inhomogeneous plasma in adiabatic expansion (e.g. Corbel 1999, and references therein).

Let us now examine the high energy part of the optically thin synchrotron spectrum, which is here thought to be at $\lambda \leq$ 90 μm. If the fluxes measured at 90 and 60 μm correspond to optically thin emission (index ≤−0.6) then the electron energy distribution is a power-law with $\delta \geq 2.2$.

In the optically thin case, if B is uniform the degree of linear polarization is: $\Pi_{\rm thin} = \frac{\delta+1}{\delta+7/3}$. In the optically thick case, it is $\Pi_{\rm thick} = \frac{3}{6\delta+13}$. Whereas $\Pi_{\rm thin}$ is high for typical values of δ, $\Pi_{\rm thick}$ is rather low. Note that the expansion of the synchrotron emitting plasma cloud may be accompanied by a rotation of the electric vector.

The estimates made in the former sections suggest that $\delta \geq 2$. The degree of linear polarization in the optically thick case should thus be ≤12%: the linear and circular degrees of <10% found in the data between 1 and 21 cm are consistent with this estimate; in order to lead to a degree of polarization much lower than predicted by theory, either the magnetic field (strength and direction) should vary strongly within the source and with time, or the synchrotron radiation should have travelled through an inhomogeneous medium. In the optically thin case, the degree should be 69%, but, to date, no polarization degree has been measured below 1 cm.

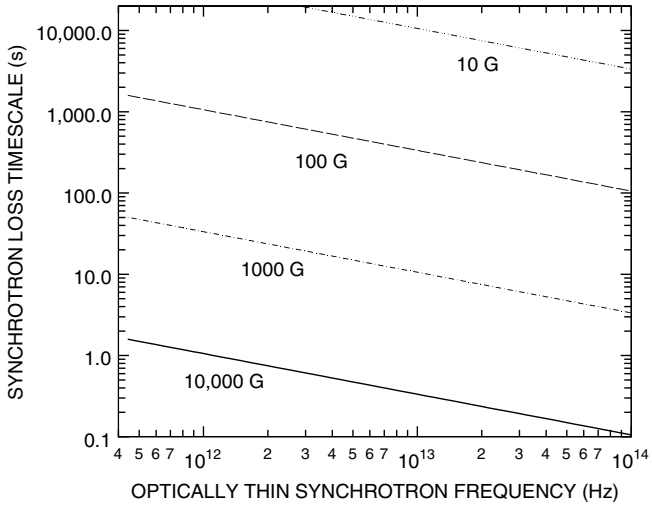

Fig. 7. Synchrotron loss timescale (in seconds) as a function of the characteristic synchrotron frequency $\nu_{\rm cr}$ (in Hz), plotted for $\nu >$ 394 GHz ($\lambda <$ 761 μm).

At high energies, several processes affect the predicted synchrotron spectrum (e.g. Rybicki & Lightman 1979; Melrose 1994). We shall now investigate these aspects.

a) Losses via synchrotron "versus" losses via adiabatic expansion

Synchrotron spectra evolve due to losses by synchrotron radiation and adiabatic expansion. The BDC model contains many assumptions, so that it is important to search for measurable parameters which can result in an independent test for the model parameters. The fact that AE Aqr exhibits radio flares, allows us to infer system parameters from the flare timescales. Whereas the rise of each flare can be associated with an acceleration process, the decay of the flare can be seen either as due to energy losses (betatron or synchrotron losses), or, due to a decrease in the magnetic field strength due to expansion. The electron characteristic synchrotron loss time (or variability timescale, or the age of the source), that is, the time for the electron to loose half of its initial energy E_o is $t_{\rm syn}(s) \simeq \frac{10^{12}}{(B^3\nu_{\rm cr})^{1/2}} \simeq \frac{5\times10^8}{\gamma B_\perp^2}$, and we have $t_{\rm adia.expans.} = r/v$. Whereas the betatron loss timescale scales with electron energy E, the synchrotron loss timescale scales as E^2, so that the latter loss process dominates the former at high energies. Furthermore, at high energies, the synchrotron loss timescale is also expected to dominate the timescale for magnetic field decay due to expansion. It is therefore useful to explore the parameter space where synchrotron losses may be dominant, or, at least comparable to betatron losses.

Figure 7 shows $t_{\rm syn}$ as a function of the characteristic synchrotron frequency $\nu_{\rm cr}$, plotted for $\nu >$ 394 GHz ($\lambda <$ 0.761 mm). For atypical field strength of B = 1000 G,

we see that the variability timescale must be smaller than 1 min above the minimum turnover frequency of 394 GHz (betatron losses, if important, will only tend to reduce this timescale). Furthermore, acceleration near the white dwarf (where the field may be as large as 10^4 G) may result in variability timescales of a few seconds. If $\nu_{\rm cr}(E_{\rm HIGH}) \geq 3 \times 10^{12}$ Hz (90 μm), then for B = 1, 10, 100, 1000 and 10^4 G, we would find respectively $t \leq 3.65$ days, 2.8 h, 5 min, 10 s and 0.3 s. It is clear that for fields stronger than several hundred G, no variability can be seen at 90 μm given the relatively long ISOPHOT integration time (118 s), since all possible variability is then smeared out. Shorter integrations must be achieved if we want to learn more about the system, but the signal-to-noise ratio may then be a problem.

The losses by synchrotron radiation steepen the power-law electrons energy distribution at very high energies, giving:

$$N(E) \propto E^{-(\delta+1)}.$$

At frequencies $> \nu_{\rm cr}(E_{\rm HIGH})$(Hz), which decreases with time, the optically thin spectrum thus steepens, changing its spectral index from $-(\delta-1)/2$ to $-(2\delta+1)/3$. The frequency $\nu_{\rm cr}(E_{\rm HIGH})$ is most probably in the infrared for AE Aqr. If $\nu_{\rm cr}(E_{\rm HIGH}) \geq 3 \times 10^{12}$ Hz (90 μm), then the estimated spectral index is $-(2\delta+1)/3 \leq -0.6$, which leads to $\delta \geq 0.4$. Again, if we wish to study the evolution of plasmoids, time resolved spectra are necessary.

b) Losses by Inverse Compton Scattering

In addition to synchrotron losses, losses by Inverse Compton Scattering (ICS) may also come into play: collisions of low energy "target" photons (radio to optical) with relativistic electrons transfer energy to photons (ultraviolet to γ-rays). They also make the higher energy electrons loose more energy. U being the energy density of the radiation field, for $\nu > \nu_{\rm cr}(E_{\rm HIGH})$ (GHz) $\simeq 4B_{\perp}/(Ut_{\rm ICS})^2$, with U in erg cm^{-3}, the ratio of loss times is $t_{\rm ICS}/t_{\rm syn} \propto B^2/U$: if the magnetic energy density $B^2/(2\mu_o)$ is $<U$, then the inverse Compton scattering losses dominate over synchrotron losses.

Inverse Compton Scattering in the Thomson limit gives the same spectral index as synchrotron emission (i.e. $-(\delta-1)/2$), unless the center-of-mass energy (electron and target photon) is more than the electron rest mass energy. For AE Aqr and electron energies below a few hundred MeV, the center-of-mass energy is well below the electron rest mass, in which case the spectral index for inverse Compton scattering is the same as for synchrotron (e.g. Melrose 1994). Only for TeV electrons do we expect the steepening relative to synchrotron spectra (i.e. the extreme Klein-Nishina effect).

Inverse Compton emission would dominate over synchrotron in the orbit of AE Aqr at the distance r from the white dwarf where:

$B^2/8\pi < L_{\rm opt/uv}/4\pi r^2 c$ where $L_{\rm opt/uv}$ is the radiated luminosity in both the optical and the ultraviolet and $L_{\rm opt/uv}/4\pi r^2 c$ is the energy density of the photons arriving on a medium located at a distance r from the UV/optical source, assumed to be the white dwarf.

Rewriting this in terms of the magnetic moment, we can show that inverse Compton emission will dominate synchrotron losses if the radius exceeds:

$$r > \left[c\mu^2/2L_{\rm opt/uv}\right]^{1/4} \text{ cm}.$$

For $\mu = 10^{32}$ G cm^3 and $L_{\rm opt/uv} = 10^{32}$ erg/s, we get inverse Compton domination for

$$r > 3.5 \times 10^{10} \text{ cm} = 0.2a.$$

On the other hand, below a distance of $\sim 0.2a$ from the white dwarf, synchrotron losses will dominate over ICS.

5. Summary and conclusions on the time-averaged emission from AE Aquarii

5.1. In the near infrared: mainly secondary star spectrum, some accretion flow contribution, and maybe some weak cyclotron emission from post-shock accretion flow near the white dwarf

AE Aqr had not been detected at 3.6 μm $< \lambda <$ 761 μm until now. In this paper, we have presented the first flux measurements of AE Aqr ever made on a large range of infrared wavelengths. It has been measured by ISOCAM from 4.956 to 6.968 μm, with fluxes which fit in well with the former measurements in the *JHKL* bands, but it is difficult to distinguish the proportion of flux which comes from the red dwarf secondary versus the accretion stream and some possible weak cyclotron emission from the post-shock accretion flow close to the magnetised white dwarf. At 7.3 μm, ISOPHOT-P has measured a flux slightly higher than at $\sim$7.0 μm (ISOCAM), but with an uncertainty which suggests a common origin for the two emissions.

5.2. Near to far infrared data: Dust unlikely; no (dominating) Circum-Binary disc

The IRAS data (recorded in 1983) have been reprocessed and bring stronger constraints than in the past: the upper limit at 100 μm is in agreement with our other results, and AE Aqr was detected at 60 μm at a flux level lower than at 90 μm and of the same order of magnitude as the upper limit at 25 μm, which is lower than that at 12 μm. The fluxes detected with ISOPHOT-C at 90 μm and IRAS at 60 μm, and the upper limit at 170 μm are of the same order of magnitude as the average flux at 761 μm, which suggests that AE Aqr has a flat average spectrum from $\sim$60 μm to $\sim$761 μm, unless it has two disconnected sources of emissions. Together with the upper limit at 10 μm (BSC85), our results suggest that the flux of AE Aqr decreases with wavelength from 90 μm down to $\sim$7.3 μm, following possibly a power-law of index ≤ -0.6. Therefore, the presence of thermal emission from dust grains, which may normally be between 1 and 100 μm, seems to be very unlikely. We have discarded the Circum-Binary disc predicted by DTS, or,

if any CB disc is present in AE Aqr, its parameters are substantially lower than those predicted by DTS, so that its highest flux measurement could be the flux measured at 7.3 μm, and it would be dominated by another emission process at $\lambda \geq 60\,\mu$m.

5.3. At $\lambda > 7$ μm: Magneto-bremsstrahlung from thermal and non-thermal electron energy distributions from a source of initial diameter 1/3 of the binary, rather than thermal bremsstrahlung from a huge source of 1 au diameter

In order to identify the mechanism leading to the far infrared emission, we have started from the usual assumptions that it comes from a spherical source emitting isotropically, whose diameter is of the order of the binary separation: this suggested a thermal emission process. A thermal electron energy distribution of temperature 575 K in a sphere of diameter of 1 astronomical unit and of electron number density of 4×10^8 cm^{-3} could lead to thermal bremsstrahlung to account for the emission from $\sim$7 μm to $\sim$the sub-millimetre, but it is difficult to imagine how such a large plasma sphere could be fed only by a mass loss rate of $\sim 10^{17}$ g/s, which is thought to be mainly in the orbital plane of the binary. Such a volume could contain a small, non-thermal source of magneto-bremsstrahlung which dominates in radio (the density of the large thermal source being sufficiently low to let the radio emission out).

A more realistic explanation is that a rather small volume (diameter below a third of the binary separation) of both thermal and non-thermal plasma is the source of magneto-bremsstrahlung peaking between $\sim$90 and $\sim$761 μm: it is optically thin to $\sim$7 to 90 μm infrared photons and optically thick to photons of $\lambda \geq 761$ μm. In order to proceed from an initial mid infrared source of both thermal and non-thermal gyro-synchrotron emission to a radio non-thermal synchrotron source, it is necessary that the mid infrared source is energised (cf. Meintjes & Venter 2003); hence, the mid infrared flare profiles are not expected to be correlated with the radio ones.

5.4. Future investigations

Measurements definitely need to be performed again from the infrared to the radio domains. A more thorough work would ideally be the study of the time variations of AE Aqr flux thanks to simultaneous and sensitive observations with high resolutions over a complete orbital period from $\lambda \simeq$ a few μm to metric wavelengths – this latter domain to search for any of the predicted change of the synchrotron optically thick slope, which provides information on the radio source and the environment. Other characteristics of the various processes should also be tested in the future (e.g. the degrees of polarization).

In addition, combined observations in radio/far infrared, low energy gamma-rays (by INTEGRAL) and medium energy gamma-rays (by GLAST) will allow us to disentangle the different emission mechanisms. From this, we will be able to measure B, the radius of emission, the particle density n_e, and the electron spectrum.

Acknowledgements. We are very grateful to Dr. M. Haas for kindly making the first processing of our ISOPHOT-C data, which needed a non standard processing and were reported in Abada-Simon et al. (1999). We thank W.S. Holland (JCMT) for processing the 1993 SCUBA-JCMT data which variability is exploited in this paper. We are also grateful to P. Meintjes, A. Serber, L. Venter, P. Fedou, and A. Raoult for very useful discussions.

References

Abada-Simon, M., Lecacheux, A., Bastian, T. S., et al. 1993, ApJ, 406, 692
Abada-Simon, M., Bastian, T. S., Horne, K., et al. 1995a, in Cape Workshop on Magnetic Cataclysmic Variables, ed. D. A. H. Buckley & B. Warner, ASP Conf. Ser., 85, 355
Abada-Simon, M., Bastian, T. S., Bookbinder, J. A., et al. 1995b, Lect. Notes Phys., 454, 268
Abada-Simon, M., Bastian, T. S., Fletcher, L., et al. 1996, ASP Conf. Ser., 93, 182
Abada-Simon, M., Mouchet, M., Aubier, M., et al. 1999, in The Universe as Seen by ISO, ed. P. Cox, & M. F. Kessler, ESA-SP, 427
Abraham, P., Acosta-Pulido, J. A., Klaas, U., et al. 2003, ESA SP-481, ed. L. Metcalfe, A. Salama, S. B. Peschke, & M. F. Kessler, 89
Altenhoff, W. J., Thum, C., & Wendker, H. J. 1994, A&A, 281, 161
Bastian, T. S., Beasley, T., & Bookbinder, J. A. 1996, ApJ, 461, 1016
Bastian, T. S., Dulk, G. A., & Chanmugam, G. 1988, ApJ, 324, 431 (BDC)
Beardwood, R. J., & Melrose, D. B. 1990, Proc. ASA, 8 (3), 283
Beichman, C. A., Neugebauer, G., Habing, H. J., et al. 1988, IRAS Catalogs and Atlases: Explanatory Supplement (Washington, DC: GPO)
Berriman, G., Szkody, P., & Capps, R. W. 1985, MNRAS, 217, 327 (BSC85)
Bowden, C. C. G., Bradbury, S. M., Chadwick, P. M., et al. 1992, Astroparticle Physics, 1, 47
Casares, J., Mouchet, M., Martinez-Pais, I. G., & Harlaftis, E. T. 1996, MNRAS, 282, 182
Cesarsky, C. J., Abergel, A., Agnèse, P., et al. 1996, A&A, 315, L32
Chanmugam, G. 1987, Ap&SS, 130, 53
Clavel, J., Schulz, B., Altieri, B., et al. 2000, A&A, 357, 839
Corbel 1999, Ph.D. Thesis, Université Pierre et Marie Curie (Paris VI), 112
Cordova, F. A., Mason, K. O., & Hjellming, R. M. 1983, PASP, 95, 69
Dhillon, V. S., & Marsh, T. R. 1995, MNRAS, 275, 89
Dubus, G., Taam, R. E., & Spruit, H. C. 2002, ApJ, 569, 395 (DTS)
Dulk, G. A. 1985, ARA&A, 23, 169
Gabriel, C., Acosta-Pulido, J., Heinrichsen, I., Morris, H., & Tai, W.-M. 1997, Proc. of the ADASS VI Conference, ed. G. Hunt, & H. E. Payne, 108
de Jager, O. C., Meintjes, P. J., O'Donoghue, D., & Robinson, E. L. 1994, MNRAS, 267, 577
Kessler, M. F., Steinz, J. A., Anderegg, M. E., et al. 1996, 315, L27
Kuijpers, J., Fletcher, L., Abada-Simon, M., et al. 1997, A&A, 322, 242
Lamb, D. Q. 1988, in Polarised Radiation of Circumstellar Origin, ed. G. V. Coyne et al., Vatican Observatory, 151
Lamb, D. Q., & Patterson, J. 1983, in IAU Coll. 72, ed. M. Livio, & G. Shaviv (Dordrecht: Reidel Publishers Company), 229
Lemke, D., Klaas, U., Abolins, J., et al. 1996, A&A, 315, L64
Li, J., Wickramasinghe, D. T., & Wu, K. 1995, MNRAS, 20,
Lin, D., & Liang, E. P. 1999, A&A, 341, 954

Meintjes, P. J., & Venter, L. A. 2003, MNRAS, 341, 891
Meintjes, P. J., Raubenheimer, B. C., de Jager, O. C., et al. 1992, ApJ, 401, 325
Meintjes, P. J., de Jager, O. C., Raubenheimer, B. C., et al. 1994, ApJ, 434, 292
Melrose, D. B. 1994, in Plasma Astrophysics, ed. J. G. Kirk, D. B. Melrose & E. R. Priest (Springer-Verlag)
Müller, T. G. 2000, in ISO Beyond Point Sources, ed. R. Laureijs, K. Leech, & M. F. Kessler, ESA SP-455
Newell, S. J., Garrett, M. A., & Spencer 1998, MNRAS, 293, 17
Ogley, R. N., Bell Burnell, S. J., Spencer, R. E., et al. 2001, MNRAS, 326, 349
Pacholczyk, A. G. 1970, Radio Astrophysics – Nonthermal processes in galactic and extragalactic sources (San Francisco: Freeman & Company)
van Paradijs, J., Kraakman, H., & van Amerongen, S. 1989, A&AS, 79, 205
Perryman, M. A. C., Lindegren, L., Kovalevsky, J., et al. 1997, A&A, 323, L49
Pooley, G. G., & Fender, R. P. 1997, MNRAS, 292, 925
Schenker, K., King, A. R., Kolb, U., et al. 2002, MNRAS, 337, 1105
Schulz, B., Huth, S., Laureijs, R. J., et al. 2002, A&A, 381, 1110
Stetson, P. B. 1987, PASP, 99, 191
Stockman, H. S., Schmidt, G. D., Berriman, G., et al. 1992, ApJ, 401, 626
Szkody, P. 1977, ApJ, 217, 140
Tanzi, E. G., Chincarini, G., & Tarenghi, M. 1981, PASP, 93, 68
Ulich, B. L. 1981, AJ, 250, 341
Wynn, G. A., King, A. R., & Horne, K. 1997, MNRAS, 286, 436 (WKH97)